European Journal of Radiology 110 (2019) 175–180

Contents lists available at ScienceDirect

European Journal of Radiology

journal homepage: www.elsevier.com/locate/ejrad

Intermodel disagreement of myocardial blood flow estimation from dynamic CT perfusion imaging

Marly van Assen[a,b], Gert Jan Pelgrim[b], Carlo N. De Cecco[a,d], J. Marco A. Stijnen[c], Beatrice M. Zaki[a], Matthijs Oudkerk[b], Rozemarijn Vliegenthart[a,b], U. Joseph Schoepf[a,*]

[a] Division of Cardiovascular Imaging, Department of Radiology and Radiological Science, Medical University of South Carolina, 25 Courtenay Drive, Charleston, SC, USA
[b] Center for Medical Imaging, University Medical Center Groningen, University of Groningen, Groningen, the Netherlands
[c] LifeTec Group, Eindhoven, the Netherlands
[d] Division of Cardiothoracic Imaging, Nuclear Medicine and Molecular Imaging, Department of Radiology and Imaging Sciences, Emory University Hospital, Atlanta, GA, USA

ARTICLE INFO

Keywords:
Computed tomography
Perfusion imaging
Myocardium
Tracer kinetic models

ABSTRACT

Purpose: To assess the intermodel agreement of different tracer kinetic models to determine myocardial blood flow (MBF) and their diagnostic accuracy in coronary artery disease (CAD) at dynamic CT myocardial perfusion imaging (CTMPI).

Methods: Three porcine hearts perfused in Langendorff mode and 15 patients with suspected CAD and perfusion single photon emission CT (SPECT) were included. Dynamic CTMPI was performed in shuttle-mode (70 kVp, 350mAs/rot) on 3rd generation dual-source CT. In porcine hearts and patients, myocardial segments (AHA-16-segment model) were drawn. Tissue attenuation curves were constructed per segment and arterial input functions were derived from the aorta. True MBF was calculated with input flow and weight of the porcine hearts. In patients, ischemic segments were based on SPECT results. MBF quantification was performed using the VPCT-software, Upslope, Extended Toft (ET), Two-compartment (TC) and Fermi models.

Results: In porcine hearts, true MBF was 1.88 (interquartile range [IQR]:1.80-2.80)mL/g/min. Diagnostic accuracy was similar for all models: 0.96, 0.99, 0.92, 0.93 and 0.96 for VPCT software, Upslope method, Fermi, ET and TC model. The VPCT software and Upslope method resulted in lower MBF (median 1.44 [1.29–1.58] and 1.39 [1.25–1.59]mL/g/min) compared to the Fermi, ET, and TC model (median values of 1.76 mL/g/min [1.36–2.44], 2.55 mL/g/min [2.20–2.92], and 1.98 mL/g/min [1.60–2.60], respectively [$p < 0.001$]). In patients, all models showed a significant difference in MBF between the 34 ischemic and 206 non-ischemic segments (p-value < 0.001).

Conclusion: Absolute MBF values are significantly different between the models and a uniform threshold could not be determined; however, diagnostic accuracy for detecting ischemia is similar.

1. Introduction

Dynamic CT myocardial perfusion imaging (CTMPI) for the evaluation of coronary artery disease (CAD) has gained interest due to technical improvements in both the hard- and software components of CT instruments [1,2]. In comparison to other imaging modalities, CTMPI offers several advantages, the most important of which being the ability to quantify myocardial blood flow (MBF). By using CTMPI in tandem with CT angiography (CTA), the morphological and functional characteristics of CAD can be evaluated within a single imaging modality [3–5].

Quantitative analysis of perfusion data reduces subjectivity and increases the accuracy of dynamic CTMPI analysis [6,7]. MBF can be quantified with CTMPI using a deconvolution method with a tracer kinetic model. The multitude of tracer kinetic models that exist describe slightly different physiological processes with varying grades of complexity [8–10]. The tracer kinetic models specifically used for the quantification of MBF based on dynamic CTMPI data are directly translated from MRI perfusion studies [9,11,12]. As expected, the wide range of models that are used in MR and CT studies result in different

* Corresponding author.
E-mail addresses: vanasse@musc.edu (M. van Assen), g.j.pelgrim@umcg.nl (G.J. Pelgrim), carlo.dececco@emory.edu (C.N. De Cecco), m.stijnen@lifetecgroup.com (J.M.A. Stijnen), zaki@musc.edu (B.M. Zaki), m.oudker@rug.nl (M. Oudkerk), r.vliegenthart@umcg.nl (R. Vliegenthart), schoepf@musc.edu (U.J. Schoepf).

https://doi.org/10.1016/j.ejrad.2018.11.029
Received 6 September 2018; Received in revised form 18 October 2018; Accepted 23 November 2018
0720-048X/ Published by Elsevier B.V.

thresholds and MBF values [13–17].

Reliable diagnosis of CAD, global ischemia, or even subclinical perfusion disturbances requires accurate MBF values in order to determine optimal thresholds [18,19]. To the best of our knowledge, there is no study comparing the different tracer kinetic models of dynamic CT myocardial perfusion in a clinical setting. Further information regarding the accuracy of CT-derived quantitative myocardial perfusion measures is needed to determine the optimal quantification method for clinical practice. In addition, we took advantage of an *ex-vivo* porcine heart model to control flow parameters and to compare calculated values to true MBF values.

Therefore, the aim of our study was to assess the intermodel agreement of different tracer kinetic models in determining myocardial blood flow (MBF) and evaluate their ability to determine hemodynamically significant CAD at dynamic CTMPI.

2. Methods and materials

2.1. Porcine hearts

Three hearts were obtained from Dutch Landrace Hybrid pigs. All protocols were in accordance with the EC regulation 1069/2009 regarding the use of slaughterhouse animal material for diagnosis and research, supervised by the Dutch Government (Dutch Ministry of Agriculture, Nature and Food Quality), and approved by the associated legal authorities of animal welfare (Food and Consumer Product Safety Authority). The transport of the hearts from the slaughterhouse to the CT system took approximately 3-4 h, during which physiological preservation of the hearts was optimal. The three porcine hearts were perfused using an isolated ex-vivo heart model (Physioheart TM, LifeTec Group, Eindhoven, The Netherlands) in Langendorff mode [9]. Blood from a venous reservoir was pumped into the coronaries by means of retrograde flow through the aorta, using a centrifugal pump (BioMedicus, Medtronic, Minneapolis, MN, USA). The aortic valve was closed due to the retrograde pressure on the valve, ensuring that all circulating blood passed through the coronary arteries. A more detailed description regarding the model's application in CT-based imaging has been previously published [10].

The porcine hearts were weighed after the experiments. True MBF was used as the reference MBF value in order to evaluate the accuracy of the different model's calculated values. True MBF was obtained based on the weight (g) of the heart and the input flow (mL/min) using the following equation:

$$\text{MBFtrue} = (\text{Input Flow}) / (\text{Heart weight}) \quad (1)$$

2.2. Patients

The study protocol was approved by our IRB and all patients provided written informed consent. We recruited adult patients who presented to our institution with a clinical history and/or symptoms suspicious for CAD and who underwent rest-stress perfusion single photon emission CT (SPECT) imaging. Subsequently, they underwent coronary CTA and dynamic stress CTMPI within 30 days of SPECT. The first 15 consecutive patients who met the inclusion criteria were prospectively enrolled in the study.

2.3. CT-protocol porcine hearts

A third generation dual source CT system (SOMATOM Force, Siemens Healthineers, Forchheim, Germany) was used to perform dynamic CTMPI on the porcine hearts. A baseline non-contrast scan was performed at 70 kV with 20mAs to confirm the field of view (FOV). An electrocardiography (ECG)-triggered shuttle mode was used for the dynamic CTMPI acquisition with the following parameters: tube voltage of 70 kV, tube current time product of 350mAs per rotation, gantry rotation time of 250 ms, and a z-range of 10.2 cm. The shuttle mode scans were performed during end-systole. For the dynamic CTMPI scans, 15 mL of ioxaglate (Hexabrix, 320 mg/mL, Guerbet, Paris, France) contrast agent was injected at a flow rate of 3 mL/s. The scan protocol was initiated 5 s prior to injection of contrast agent. Data were collected over a 60 s time period during first pass inflow and outflow of iodine through the myocardium. The inflow tube of the perfusion system was looped through the FOV of the perfusion scans, acting as a substitute aorta. The arterial input function (AIF) was derived from the substitute aorta and is essential for the quantification of MBF.

2.4. CT-protocol patients

All patients underwent dynamic stress CTMPI, also using 3rd generation dual source CT. Imaging was performed in ECG-triggered shuttle mode in which the table shifted between two z-positions of the heart to allow coverage of the entire left ventricle. Imaging started approximately 90 s after a bolus injection of Regadenoson (Lexiscan™, Astellas Pharma US, Deerfield, IL) at 0.4 mg per 5 mL, immediately followed by a 10 cc saline flush. Contrast administration began approximately 80 s after the Regadenoson bolus to allow the contrast to reach the heart at the moment of maximal hyperemia. A total of 40–50 mL of 370 mgI/mL iopromide (Ultravist; Bayer Healthcare, Wayne, NJ) at a flow rate of 4–6 mL/s was administered. Data were acquired for 30 s at 80–100 kV, a gantry rotation time of 280 ms, and a tube current of 300 mAs per rotation. Images were acquired during the end systolic phase. A total of 14–15 images were obtained for each patient. Patients were asked to hold their breath for a minimum of 20 s, but preferably thirty. They were instructed that when it became difficult to hold their breath small shallow breathing was preferred.

2.5. Data analysis

Dynamic CT MPI data were reconstructed with a section thickness of 3 mm and a 2 mm increment with a medium smooth convolution kernel (B30). CT perfusion images were analysed on a dedicated workstation using commercially available software (Siemens, Syngo Volume Perfusion™). After motion correction and 4D noise reduction, extraction of the AIF and tissue attenuation curves (TAC) for each myocardial segment was performed. The American Heart Association (AHA) 16-segment model was used to classify the myocardial segments at basal, mid-ventricular, and apical short axis-slices. The software calculated MBF for every segment with extracted curves. Volume Perfusion CT Myocardium software (VPCT) software calculates MBF in mL/100 mL/min; this was recalculated to MBF in mL/g/min using a 1.05 conversion factor to correspond with the MBF values from the other models. In patients, ischemic segments were identified based on stress perfusion SPECT images by a radiologist with 11 years of experience in cardiac imaging (__). Very small SPECT defects (< 10%) and artifacts were considered as normal segments at the discretion of the radiologist. In case of high uncertainty segments were excluded from analysis.

2.6. Tracer kinetic models

The AIF and TAC from each of the 16 myocardial segments were analyzed using an in-house Matlab script (Matlab R2014b, Mathworks Inc., Natick, MA). MBF was calculated using the Upslope method, extended Toft (ET), two compartment (TC), and Fermi model (Table 1). The AIF and TAC curves were corrected for baseline differences and contrast build-up, and subsequently resampled to correct for non-uniform temporal sampling rates caused by heart rate variations. The fitting procedure was performed with a nonlinear least-squares solver using a trust-region-reflective algorithm. The fitting procedure was constrained to ensure that estimated flow parameters were within physiological range (Flow 0.1–10 mL/g/min).

Table 1
Model functions.

Model	Fitting parameters	Model function	Restrains
Upslope	–	$\frac{Maximum\ Upslope\ (TAC)}{Maximum\ Value\ (AIF)}$	–
Fermi	MBF (F) MTTc and k do not have a physiological meaning	$IRF(t) = \frac{F}{exp^{k(t-MTTc}+1}$	Only Upslope TAC
Extended Toft	Indirect MBF(Ktrans), extracellular extravascular space volume fraction (vp), intravascular plasma volume fraction (ve)	$IRF(t) = Ktrans * exp^{-\frac{Ktrans}{ve}(t)} + vp\,\partial(t)$	Ktrans instead of flow (F)
Two compartment	MBF(F), extracellular extravascular space volume fraction (vp), extracellular extravascular space exchange rate (PS), intravascular plasma volume fraction (ve)	$IRF(t) = F * exp^{-\frac{F}{vp}(t)} + PS * exp^{-\frac{PS}{ve}(t)}$	

IRF = impulse response function describing the model response.

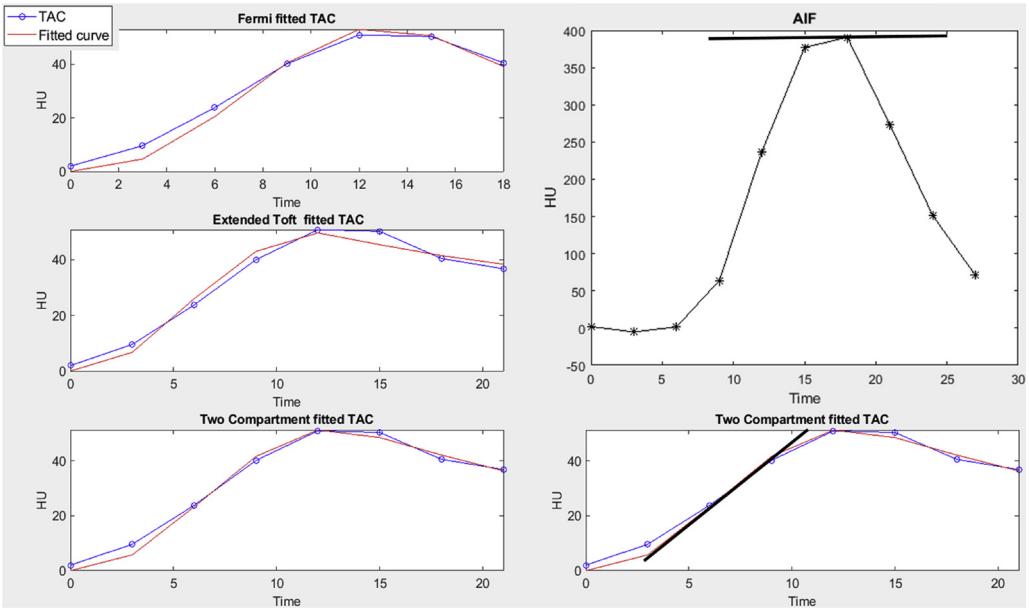

Fig. 1. The left three panels represent the measured TAC curves (blue) and the fitted curves (red) with the Fermi, Extended Toft and Two compartment model, respectively. The right panels visualize the use of the Upslope model, using the maximal value of the AIF curve (upper panel) and the maximal upslope of the TAC curve represented by a two compartment model (lower panel).

The Upslope method uses a combination of quantitative and semi-quantitative methods. The TAC curve is described by a two-compartment model in which the peak of the AIF and the maximal upslope of the TAC determine MBF, see Fig. 1.For the fitting procedure of the Fermi function, only the upslope of the TAC was selected. The models are described in more detail in previous publications [8–10,17,20,21]. The VPCT software, extensively validated for the detection of ischemia [22–24], uses a Patlak method which is based on a combination of an upslope method and a two compartment model, similar to our Upslope method.

2.7. Statistical analysis

Statistical analysis was performed using SPSS 23 (IBM Corp, Armonk, NY, USA). Calculated MBF values were compared with true MBF values in porcine hearts to evaluate which model provides the most accurate MBF values. A Kruskal-Wallis test was used to test for differences between the models in porcine hearts. Appropriate statistical analyses (t-test for normally distributed data, Whitney Mann-U test for non-normal data distribution) were used to compare CT-based MBF between different models in both the porcine hearts and patients, as well as between ischemic and non-ischemic segments in patients. Pearson's correlation coefficient was used to determine the correlation between the models. Bland-Altman plots were used to show agreement between the different models and associated mean biases were calculated. Receiver operating characteristic (ROC) curves were generated using MBF as the continuous variable. The area under the ROC curve (AUC) was calculated for each model and optimal MBF cut-off values for the ROC curves.

3. Results

3.1. Porcine hearts

The true MBF ranged from 1.78 mL/g/min to 2.80 mL/g/min for the three hearts. A total of 48 segments were analyzed. Median calculated MBF values were 1.44 (interquartile range [IQR] 1.29–1.58) mL/g/min, 1.39 (1.25-1.59) mL/g/min, 1.76 (1.36–2.44) mL/g/min, 2.55 (2.20–2.92) mL/g/min and 1.98 (1.60–2.60) mL/g/min for the VPCT, Upslope, Fermi, ET, and TC method, respectively. MBF values generated with the different models were significantly different (all $p < 0.001$) for all models accept the VPCT and upslope model. The VPCT and Upslope method provided the lowest values and thereby underestimated the true MBF, while the ET model consistently gave the highest values and overestimated the true MBF. The TC model resulted in the smallest difference (0.36 mL/g/min) compared to the true MBF values and was therefore the most accurate. Fig. 1 provides examples of the fitting procedure for the different models. Table 2 shows the median values for MBF calculated with the different models for the three porcine hearts.

3.2. Patients

The study included a total of 15 patients (median age, 69 years), 3 of whom were male. Of these patients, 8 were without ischemia and 7 patients had at least one ischemic segment according to SPECT. Fig. 2 shows an example of CTMPI studies of two patients, one with ischemia and one without ischemia. None of the patients showed any sign of myocardial infarction based on analysis of the rest and stress SPECT

Table 2
MBF measurements in porcine hearts.

Demographic	Median (IQR) or n (%)
Age, years	69 (60-77)
Male, n	3 (20.0)
BMI, kg/m^2	28.9 (25.3-32.8)
Caucasian Ethnicity, n	11 (73.3)
Hypertension, n	14 (93.3)
Hyperlipidaemia, n	15 (100)
Diabetes, n	6 (40.0)
Smoking, n	7 (46.7)

Values are given as n (%) or as median (IQR). ET; extended Toft, TC; two compartment.

Table 3
PATIENT CHARACTERISTICS.

Demographic	Median (IQR) or n (%)
Age, years	69 (60-77)
Male, n	3 (20.0)
BMI, kg/m^2	28.9 (25.3-32.8)
Caucasian Ethnicity, n	11 (73.3)
Hypertension, n	14 (93.3)
Hyperlipidaemia, n	15 (100)
Diabetes, n	6 (40.0)
Smoking, n	7 (46.7)

Values are given as n (%) or as median (IQR).

images. Median radiation dose of the CTMPI acquisition was 3.44 mSv (IQR: 2.55–4.83). Patient characteristics are presented in Table 3. A total of 240 myocardial segments in stress acquisitions were analyzed. Of those 240 segments, 34 were considered ischemic based on SPECT image analysis.

Overall MBF for all combined segments was 1.60 (1.22–2.03), 1.61 (1.27–2.00), 3.34 (2.42–4.86), 4.22 (2.74–5.34), and 3.95 (2.79–4.90) mL/g/min for the VPCT software, Upslope method, Fermi, ET, and TC model, respectively. Table 4 shows the intermodel comparison of the overall MBF values between the five models. The VPCT software and the Upslope method, both based on the same mathematical principle, showed similar MBF values. These models also showed the lowest absolute MBF values. All other models showed significantly different MBF estimations (all $p < 0.001$). In accordance with results from the porcine hearts, the ET model provided the highest MBF values. Variation between segments was lowest using the VPCT and upslope methods and highest with the ET model.

Models demonstrated moderate to excellent correlation, with Pearson coefficients ranging between 0.613-0.934. The strongest correlation was found between the Fermi and TC models ($r = 0.934$; p-value < 0.001), whereas the weakest correlation was found between VPCT software and the ET model ($r = 0.613$; p-value < 0.001).

Table 4
Overall MBF values and intermodel agreement.

Overall MBF (Ml/g/min)	VPCT 1.60 (1.22-2.03)	Upslope 1.61 (1.27-2.00)	Fermi 3.34 (2.42-4.86)	ET 4.22 (2.74-5.34)	TC 3.95 (2.79-4.90)
	Absolute Mean Difference	P-value Mean Difference	Pearson's Correlation	P-value Correlation	
VPCT-Upslope	−0.021	0.263	0.860	< 0.001	
VPCT-Fermi	−1.926	< 0.001	0.627	< 0.001	
VPCT-ET	−2.392	< 0.001	0.613	< 0.001	
VPCT-TC	−2.200	< 0.001	0.655	< 0.001	
Upslope-Fermi	−1.905	< 0.001	0.797	< 0.001	
Upslope-ET	−2.371	< 0.001	0.783	< 0.001	
Upslope-TC	−2.180	< 0.001	0.829	< 0.001	
Fermi-ET	−0.466	< 0.001	0.855	< 0.001	
Fermi-TC	−0.275	< 0.001	0.934	< 0.001	
ET-TC	0.191	< 0.001	0.921	< 0.001	

Values are given as n (%) or as median (IQR). ET; extended Toft, TC; two compartment.

All models showed a significant difference between MBF of ischemic and non-ischemic segments (p-value < 0.001). Table 5 summarizes the diagnostic performance of all 5 models. Diagnostic accuracy was 0.96,

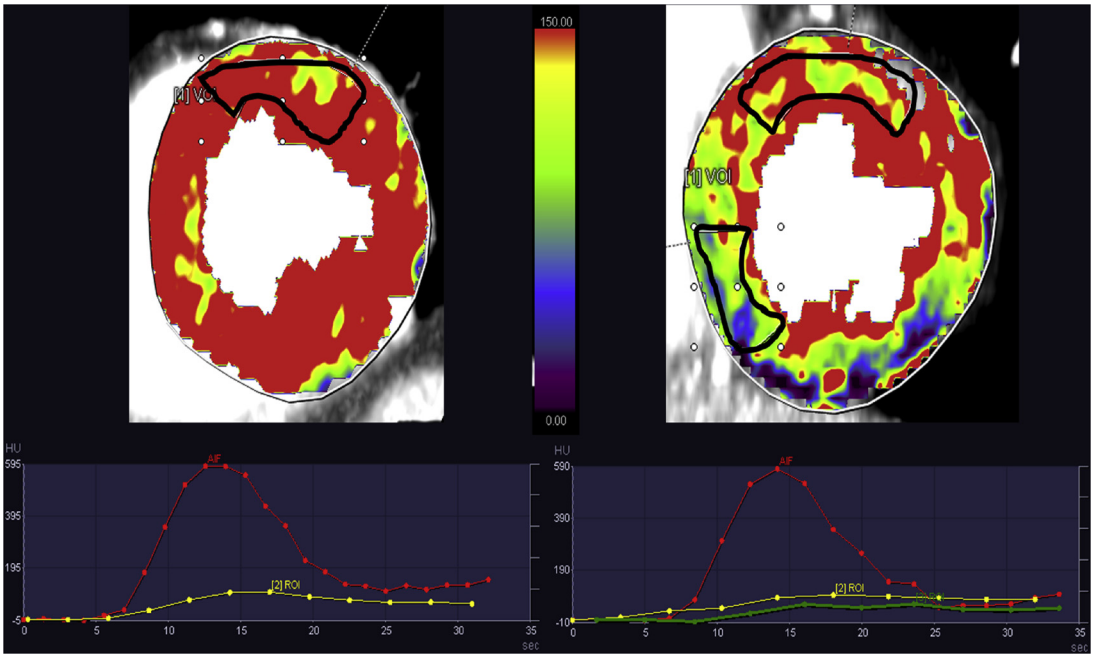

Fig. 2. On the left the midventricular slice of a patient without ischemia, where the AIF (red) and the TAC (yellow) are presented. On the right, the midventricular slice of a patient with confirmed ischemia according to the SPECT acquisition in the mid-septal and mid-inferior segments. From this patient, the AIF curve is represented (red) along with two TAC, one from the non-ischemic mid-lateral regions (yellow) and one from the ischemic region (green). The ischemic TAC is clearly lower than the non-ischemic TAC.

Table 5
Myocardial Blood flow values for ischemia detection.

	VPCT	Upslope	Fermi	ET	TC
Non-Ischemic MBF (n = 206)	1.68 (1.44-2.08)	1.71 (1.43-2.08)	3.62 (2.74-5.05)	4.63 (3.40-5.46)	4.24 (3.36-4.99)
Ischemic MBF (n = 34)	0.83 (0.67-0.99)	0.83 (0.74-0.93)	1.54 (1.13-2.00)	1.81 (1.40-2.59)	1.72 (1.29-2.38)
p-value	< 0.001	< 0.001	< 0.001	< 0.001	< 0.001
AUC	0.956	0.990	0.922	0.931	0.963
DeLong	–	0.149	0.342	0.460	0.761
Optimal threshold (mL/g/min)	1.05	1.09	2.16	2.97	2.55

Values are given as n (%) or as median (IQR).

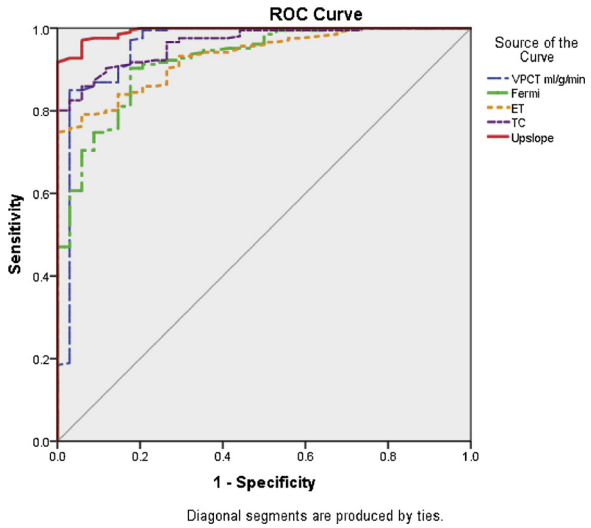

Fig. 3. The ROC curves are depicted for the VPCT software, the upslope, Fermi, Extended Toft (ET) and Two Compartment (TC) model.

0.99, 0.92, 0.93 and 0.96 for the VPCT software, Upslope method, Fermi, ET, and TC model, respectively. The optimal threshold for detecting lesion-specific ischemia was determined for each model, and represented in Table 4. Only the VPCT software and Upslope method showed similar threshold values. ROC curves with corresponding AUCs are provided for each model with SPECT as a reference standard in Fig. 3.

4. Discussion

This study evaluated dynamic CTMPI-based MBF calculation using 5 tracer kinetic models. First, we used three porcine hearts with known true MBF values to examine the accuracy of each model in quantifying absolute MBF. Subsequently, we evaluated the agreement between models in 15 patients, as well as the ability of each model to detect myocardial ischemia. Results demonstrated that the diagnostic performance of quantitative MBF measurements is not affected by the choice of tracer kinetic analysis method when measuring stress MBF. However, the absolute MBF values are significantly different between the models, with the TC model providing the most accurate MBF values when compared to the true MBF found in porcine hearts. Notably, a uniform MBF threshold could not be determined; the MBF values calculated by the different models cannot be compared for diagnostic purposes.

Currently, the reference standard for quantitative measurements of MBF is positron emission tomography (PET), reporting normal stress MBF values ranging between 3 and 5 mL/min/g [25–27]. Dynamic CTMPI has been found to underestimate MBF, with reported MBF values between 1.0 and 1.4 mL/min/g [7,28–30]. In a simulation study evaluating the effects of temporal sampling, Ishida et al. reported an underestimation of MBF by 23–41% using CT-measured values compared to true values [31]. Most clinical studies regarding dynamic CTMPI and MBF quantification use a Patlak model, with the VPCT software most commonly used. Another reason for the underestimation of CTMPI-based MBF values, aside from the limited temporal sampling rate of CTMPI, is the nature of the Patlak-based methods (VPCT software/Upslope method), which calculate the transfer coefficient (K1-Patlak) equivalent instead of MBF [31].

Prior studies have examined different dynamic cardiac CT models for MBF estimation in an animal- or computation-simulation setting. In a canine study, George et al. compared a two-compartment model and two versions of an upslope method using microsphere-based MBF as the reference standard. They concluded that all three models correlate well with the reference MBF. Although the models demonstrated a strong correlation, results did not suggest that they provide accurate quantitative estimates of MBF [21]. In a simulation study, Binschadler et al. [32] demonstrated that the upslope model is a suboptimal method for quantifying absolute MBF. In addition, the authors concluded that the three quantitative models they tested, one of which was a two-compartment model, showed no MBF estimation bias despite a substantial variance [32].

The Patlak-based methods (VPCT and Upslope) both showed the lowest variability in overall and non-ischemic MBF values. This is likely a direct consequence of the simplicity of the models and the relative inability to detect small changes. The Fermi, ET, and TC models are more complex, estimating flow or a related parameter directly from the model equation. Interestingly, the complexity of these models causes more variability in measured MBF values, but also makes them more sensitive to recognize subclinical changes or normal variations in MBF. Further research should be performed to determine the effect of stenosis severity on AIF and TAC curves.

In the current study, the Upslope model is built using the same methodology as the VPCT software. Thus, these two measurements showed a high correlation (0.860) and a small difference in absolute MBF values. The limited difference can likely be attributed to the use of different values for the parameter initialization and parameter limits given in the fitting procedure. Another reason for the difference between the two models is the way the data are sampled. Where the Upslope, TC, ET and Fermi models use data that is uniformly resampled, the VPCT software used a double sampled AIF and a single sampled TAC.

Differences in absolute values caused by the use of a different models could have great impact on the thresholds chosen to determine whether ischemia is present. Current studies focused on diagnostic performance of quantitative CT perfusion uses thresholds that are specific for their choice of model. However, as shown in this study, optimal thresholds show great variation between models and may vary between 1.05 mL/g/min and 2.97 mL/g/min. It is detrimental that in a clinical situation it is clear which model has been used to calculate MBF in order to select the appropriate threshold. Larger studies should be done on the optimized thresholds for each model. For clinical purposes a robust model with low variability could prove beneficial in cases of higher noise of artefact, while complex models might be beneficial if the goal is to detect subtle changes. Since the model is not dependent on the acquisition, an optimal model can be chosen for a specific goal after the acquisition is done.

4.1. Limitations

Relative to the total number of segments included in the patient study, a small portion was ischemic (14%). The small representation of ischemic segments may impact the diagnostic accuracy results of the different models. It should be noted that ambiguous cases, those in which SPECT imaging was not conclusive, were not included in this

study. This was done to increase the reliability of the reference standard and thereby increase the validity of our comparability study. However, as a consequence, our results cannot be considered representative of clinical diagnostic performance. Including ambiguous cases may decrease the diagnostic accuracy of these models. Since the aim of this study was to assess intermodel agreement and not clinical diagnostic accuracy, this is not considered a major limitation.

4.2. Conclusion

Absolute MBF values are significantly different between the five kinetic models; however, the diagnostic accuracy is similar. MBF values calculated by models need individual thresholds for diagnostic purposes.

Conflicts of interest and financial disclosure agreement

Dr. Schoepf receives institutional research support from Astellas, Bayer, and Siemens. Dr. De Cecco receives institutional research support from Siemens. Dr. Schoepf has received consulting fees and or speaker honoraria from Bayer, GE, Guerbet, HeartFlow Inc., and Siemens. Dr. De Cecco has received speaker honoraria from Bayer. M.A. Stijnen is a LifeTec group employee. UMCG receives institutional research support from Siemens. The other authors have no conflict of interest to disclose.

References

[1] G. Bastarrika, L. Ramos-Duran, M.A. Rosenblum, D.K. Kang, G.W. Rowe, U.J. Schoepf, Adenosine-stress dynamic myocardial CT perfusion imaging: initial clinical experience, Invest. Radiol. 45 (2010) 306–313, https://doi.org/10.1097/RLI.0b013e3181dfa2f2.

[2] M. Weininger, U.J. Schoepf, T. Henzler, D.K. Kang, G. Rowe, P. Costello, G. Bastarrika, Adenosine-stress dual-source CT dynamic myocardial volume perfusion imaging: initial clinical experience, J. Cardiovasc. Comput. Tomogr. 4 (2010) S73 http://www.embase.com/search/results?subaction=viewrecord&from=export&id=L70180820.

[3] D. Caruso, M. Eid, U.J. Schoepf, K.N. Jin, A. Varga-Szemes, C. Tesche, S. Mangold, A. Spandorfer, A. Laghi, C.N. De Cecco, Dynamic CT myocardial perfusion imaging, Eur. J. Radiol. (2016), https://doi.org/10.1016/j.ejrad.2016.07.017.

[4] I. Danad, J. Szymonifka, J. Schulman-Marcus, J.K. Min, Static and dynamic assessment of myocardial perfusion by computed tomography, Eur, Hear. J. – Cardiovasc. Imaging (2016) jew044, https://doi.org/10.1093/ehjci/jew044.

[5] M.C. Williams, D.E. Newby, CT myocardial perfusion imaging: current status and future directions, Clin. Radiol. 71 (2016) 1–11, https://doi.org/10.1016/j.crad.2016.03.006.

[6] A. Varga-Szemes, F.G. Meinel, C.N. De Cecco, S.R. Fuller, R.R. Bayer, U. Joseph Schoepf, U.J. Schoepf, CT myocardial perfusion imaging, AJR Am. J. Roentgenol. 204 (2015) 487–497, https://doi.org/10.2214/AJR.14.13546.

[7] G.J. Pelgrim, M. Dorrius, X. Xie, M.A.M. Den Dekker, U.J. Schoepf, T. Henzler, M. Oudkerk, R. Vliegenthart, The dream of a one-stop-shop: meta-analysis on myocardial perfusion CT, Eur. J. Radiol. 84 (2015) 2411–2420, https://doi.org/10.1016/j.ejrad.2014.12.032.

[8] G.J. Pelgrim, A. Handayani, H. Dijkstra, N.H.J.H.J. Prakken, R.H.J.A. Slart, M. Oudkerk, P.M.A.V. Ooijen, R. Vliegenthart, P.E.E. Sijens, P.M.A. Van Ooijen, R. Vliegenthart, P.E.E. Sijens, Quantitative myocardial perfusion with dynamic contrast-enhanced imaging in MRI and CT : theoretical models and current implementation, Biomed Res. Int. 2016 (2016), http://www.embase.com/search/results?subaction=viewrecord&from=export&id=L609230918.

[9] T.Y. Lee, Functional CT: physiological models, Trends Biotechnol. 20 (2002) 3–10, https://doi.org/10.1016/S0167-7799(02)02035-8.

[10] T.S. Koh, Tracer kinetics modeling basics: model formulation, Proc. ISMRM, (2010), pp. 1–3.

[11] M. Ingrisch, S. Sourbron, Tracer-kinetic modeling of dynamic contrast-enhanced MRI and CT: a primer, J. Pharmacokinet. Pharmacodyn. 40 (2013) 281–300, https://doi.org/10.1007/s10928-013-9315-3.

[12] M. Jerosch-Herold, Quantification of myocardial perfusion by cardiovascular magnetic resonance, J. Cardiovasc. Magn. Reson. 12 (2010) 57, https://doi.org/10.1186/1532-429X-12-57.

[13] Y. Tanabe, T. Kido, T. Uetani, A. Kurata, T. Kono, A. Ogimoto, M. Miyagawa, T. Soma, K. Murase, H. Iwaki, T. Mochizuki, Differentiation of myocardial ischemia and infarction assessed by dynamic computed tomography perfusion imaging and comparison with cardiac magnetic resonance and single-photon emission computed tomography, Eur. Radiol. (2016) 1–12 http://www.embase.com/search/results?subaction=viewrecord&from=export&id=L608199060.

[14] J.L. Wichmann, F.G. Meinel, U.J. Schoepf, G.G. Lo, Y.H. Choe, Y. Wang, R. Vliegenthart, A. Varga-Szemes, G. Muscogiuri, P.M. Canna??, C.N. De Cecco, P.M. Cannaò, C.N. De Cecco, Absolute versus relative myocardial blood flow by dynamic CT myocardial perfusion imaging in patients with anatomic coronary artery disease, Am. J. Roentgenol. 205 (2015) W67–W72, https://doi.org/10.2214/AJR.14.14087.

[15] J.L. Wichmann, F.G. Meinel, U.J. Schoepf, A. Varga-Szemes, G. Muscogiuri, P.M. Cannaò, A.D. McQuiston, Y.H. Choe, Y. Wang, C.N. De Cecco, Semiautomated global quantification of left ventricular myocardial perfusion at stress dynamic ct: diagnostic accuracy for detection of territorial myocardial perfusion deficits compared to visual assessment, Acad. Radiol. 23 (2016) 429–437, https://doi.org/10.1016/j.acra.2015.12.005.

[16] A. So, G. Wisenberg, A. Islam, J. Amann, W. Romano, J. Brown, D. Humen, G. Jablonsky, J.Y. Li, J. Hsieh, T.Y. Lee, Non-invasive assessment of functionally relevant coronary artery stenoses with quantitative CT perfusion: Preliminary clinical experiences, Eur. Radiol. 22 (2012) 39–50, https://doi.org/10.1007/s00330-011-2260-x.

[17] J.D. Biglands, D.R. Magee, S.P. Sourbron, S. Plein, J.P. Greenwood, A. Radjenovic, Comparison of the diagnostic performance of four quantitative myocardial perfusion estimation methods used in cardiac MR imaging: CE-MARC substudy, Radiology 275 (2015) 393–402, https://doi.org/10.1148/radiol.14140433.

[18] F.G. Meinel, J.L. Wichmann, U.J. Schoepf, F. Pugliese, U. Ebersberger, G.G. Lo, Y.H. Choe, Y. Wang, C. Tesche, S. Segreto, W.G. Kunz, K.M. Thierfelder, F. Bamberg, C.N. De Cecco, Global quantification of left ventricular myocardial perfusion at dynamic CT imaging: prognostic value, J. Cardiovasc. Comput. Tomogr. 11 (2017) 16–24, https://doi.org/10.1016/j.jcct.2016.12.003.

[19] R. Vliegenthart, C.N. De Cecco, J.L. Wichmann, F.G. Meinel, G.J. Pelgrim, C. Tesche, U. Ebersberger, F. Pugliese, F. Bamberg, Y.H. Choe, Y. Wang, U.J. Schoepf, Dynamic CT myocardial perfusion imaging identifies early perfusion abnormalities in diabetes and hypertension: insights from a multicenter registry, J. Cardiovasc. Comput. Tomogr. 10 (2016) 301–308, https://doi.org/10.1016/j.jcct.2016.05.005.

[20] A. Handayani, P. Triadyaksa, H. Dijkstra, G.J. Pelgrim, P.M.A. van Ooijen, N.H.J. Prakken, U.J. Schoepf, M. Oudkerk, R. Vliegenthart, P.E. Sijens, Intermodel agreement of myocardial blood flow estimation from stress-rest myocardial perfusion magnetic resonance imaging in patients with coronary artery disease, Invest. Radiol. 50 (2015) 275–282, https://doi.org/10.1097/RLI.0000000000000114.

[21] R.T. George, M. Jerosch-Herold, C. Silva, K. Kitagawa, D.A. Bluemke, J.A. Lima, A.C. Lardo, Quantification of myocardial perfusion using dynamic 64-detector computed tomography, Invest. Radiol. 42 (2007) 815–822, https://doi.org/10.1097/RLI.0b013e318124a884.

[22] G.J. Pelgrim, M. Das, S. van Tuijl, M. van Assen, F.W. Prinzen, M. Stijnen, M. Oudkerk, J.E. Wildberger, R. Vliegenthart, Validation of myocardial perfusion quantification by dynamic CT in an ex-vivo porcine heart model, Int. J. Cardiovasc. Imaging (2017), https://doi.org/10.1007/s10554-017-1171-6.

[23] F. Bamberg, R. Hinkel, F. Schwarz, T.A. Sandner, E. Baloch, R. Marcus, A. Becker, C. Kupatt, B.J. Wintersperger, T.R. Johnson, K. Theisen Da, Accuracy of dynamic computed tomography adenosine stress myocardial perfusion imaging in estimating myocardial blood flow at various degrees of coronary artery stenosis using a porcine animal model, Invest. Radiol. 47 (2012) 71–77.

[24] Y. Wang, L. Qin, X. Shi, Y. Zeng, H. Jing, U.J. Schoepf, Z. Jin, Adenosine-stress dynamic myocardial perfusion imaging with second-generation dual-source CT: comparison with conventional catheter coronary angiography and SPECT nuclear myocardial perfusion imaging, Am. J. Roentgenol. 198 (2012) 521–529, https://doi.org/10.2214/AJR.11.7830.

[25] S.A. Kajander, E. Joutsiniemi, M. Saraste, M. Pietila, H. Ukkonen, A. Saraste, H.T. Sipila, M. Teras, M. Maki, J. Airaksinen, J. Hartiala, J. Knuuti, Clinical value of absolute quantification of myocardial perfusion with (15)O-water in coronary artery disease, Circ. Cardiovasc. Imaging 4 (2011) 678–684, https://doi.org/10.1161/CIRCIMAGING.110.960732.

[26] A. Bol, J.A. Melin, J.L. Vanoverschelde, T. Baudhuin, D. Vogelaers, M. De Pauw, C. Michel, A. Luxen, D. Labar, M. Cogneau, Direct comparison of [13N]ammonia and [15O]water estimates of perfusion with quantification of regional myocardial blood flow by microspheres, Circulation 87 (1993) 512–525, https://doi.org/10.1161/01.CIR.87.2.512.

[27] G. El Fakhri, D. Ph, Reproducibility and accuracy of quantitative myocardial blood flow using 82 Rb-PET: comparison with 13 N-Ammonia, J. Nucl. Med. 50 (2011) 1062–1071, https://doi.org/10.2967/jnumed.104.007831.Reproducibility.

[28] E.Y. Kim, W.-J.J. Chung, Y.M. Sung, S.S. Byun, J.H. Park, J.H. Kim, J. Moon, Normal range and regional heterogeneity of myocardial perfusion in healthy human myocardium: assessment on dynamic perfusion CT using 128-slice dual-source CT, Int. J. Cardiovasc. Imaging 30 (2014) 33–40, https://doi.org/10.1007/s10554-014-0432-x.

[29] A. Saraste, J. Knuuti, Dynamic perfusion CT: What is normal myocardial blood flow? Eur. Heart J. Cardiovasc. Imaging 16 (2015) 288–289, https://doi.org/10.1093/ehjci/jeu211.

[30] A. Rossi, D. Merkus, E. Klotz, N. Mollet, P.J. de Feyter, G.P. Krestin, Stress myocardial perfusion: imaging with multidetector CT, Radiology 270 (2014) 25–46, https://doi.org/10.1148/radiol.13112739.

[31] M. Ishida, K. Kitagawa, T. Ichihara, T. Natsume, R. Nakayama, N. Nagasawa, M. Kubooka, T. Ito, M. Uno, Y. Goto, M. Nagata, H. Sakuma, Underestimation of myocardial blood flow by dynamic perfusion CT: explanations by two-compartment model analysis and limited temporal sampling of dynamic CT, J. Cardiovasc. Comput. Tomogr. (2016) 1–8, https://doi.org/10.1016/j.jcct.2016.01.008.

[32] M. Bindschadler, D. Modgil, K.R. Branch, P.J. La Riviere, A.M. Alessio, Comparison of blood flow models and acquisitions for quantitative myocardial perfusion estimation from dynamic CT, Phys. Med. Biol. 59 (2014) 1533–1556, https://doi.org/10.1088/0031-9155/59/7/1533.